Research Square

Preprints are preliminary reports that have not undergone peer review.
They should not be considered conclusive, used to inform clinical practice,
or referenced by the media as validated information.

Proteomic profiling of formalin-fixed paraffin-embedded specimens reveals candidate intraoperative diagnostic biomarkers for Hirschsprung disease

Shigemitsu Kojima
Gunma Children's Medical Center
Ayako Yamazaki
Gunma University Graduate School of Medicine
Masahito Yoshihara
Chiba University
Ryo Konno
Kazusa DNA Research Institute
Kenichiro Konishi
Gunma Children's Medical Center
Shinya Takazawa
Gunma Children's Medical Center
Akira Nishi
Gunma Children's Medical Center
Jun Fujishiro
The University of Tokyo
Osamu Ohara
Kazusa DNA Research Institute
Yusuke Kawashima
Kazusa DNA Research Institute
Eiichiro Watanabe
eiichiro.watanabe.riken@gmail.com

The University of Tokyo

Research Article

Keywords: Hirschsprung disease, proteomics, formalin-fixed paraffin-embedded tissue, biomarker, immunohistochemistry

Posted Date: August 31st, 2026

DOI: https://doi.org/10.21203/rs.3.rs-10765711/v1

License: This work is licensed under a Creative Commons Attribution 4.0 International License.
Read Full License

Additional Declarations: No competing interests reported.

Abstract

Background

Rare diseases such as Hirschsprung disease (HSCR) pose challenges for prospective pediatric surgical research because of limited patient numbers. Archived formalin-fixed paraffin-embedded (FFPE) tissue samples provide a valuable resource for molecular analyses without requiring additional invasive procedures. In this study, we performed a comprehensive proteomic analysis of FFPE samples from patients with HSCR to identify potential novel biomarkers for intraoperative diagnosis and further explore HSCR pathophysiology.

Methods

Proteomic analysis was performed on 45 FFPE samples from 15 patients (mean age: 6.5 ± 3.3 months, male/female = 11:4), including samples from the recto-sigmoid or long-type aganglionosis regions. The study included the aganglionic segment (AS), the transitional zone (TZ), and the normal intestine (NI) samples from each patient. Statistical significance was determined using adjusted p-values (< 0.05). Functional analysis was performed using gene set enrichment analysis.

Results

A total of 10,541 proteins were identified, of which 13 were significantly upregulated in the NI compared with the AS and TZ. Immunohistochemical validation demonstrated that catenin alpha-2 (CTNNA2), mammalian ependymin-related protein 1 (EPDR1), NAC-alpha domain-containing protein 1 (NACAD), and neural cell adhesion molecule 2 (NCAM2), previously unassociated with HSCR or gastrointestinal development, exhibited staining restricted to ganglionic regions of the large intestine.

Conclusions

These findings indicate that CTNNA2, EPDR1, NACAD, and NCAM2 may be promising candidate biomarkers for intraoperative differentiation of the NI from the TZ and AS, demonstrating the feasibility of FFPE-based proteomics for HSCR research.

Background

Rare diseases present frequent challenges in pediatric surgery, limiting the feasibility of prospective studies. Recent advances in research using formalin-fixed, paraffin-embedded (FFPE) tissue samples have created new opportunities to investigate the pathophysiology of these rare conditions.[1] In particular, liquid chromatography–mass spectrometry-based proteomic analysis of FFPE specimens has been used for more than two decades, primarily to identify molecular biomarkers in various cancers,

predominantly in adult populations.[2] Furthermore, the ability to analyze archived FFPE tissues without subjecting pediatric patients to additional invasive procedures represents a significant advancement.[3]

Hirschsprung disease (HSCR), a rare congenital disorder and one of the most common pediatric conditions requiring surgery, is characterized by the absence of parasympathetic intrinsic ganglion cells in the submucosal and myenteric plexuses of the intestine.[4] The standard surgical treatment for HSCR involves resection of the aganglionic segment (AS) and transitional zone (TZ), followed by anastomosis of the normal intestine (NI) to the anus.[4] However, distinguishing the TZ, where the aganglionic intestine transitions to NI, from NI can be challenging, particularly during intraoperative histopathologic evaluation. Even experienced pathologists may encounter difficulty differentiating these regions intraoperatively.

In this study, we performed a deep proteomic analysis of FFPE samples to identify potential novel biomarkers for intraoperative diagnosis and to further explore the pathophysiology of HSCR.

Methods

Ethics approval

This retrospective observational study was approved by the Institutional Review Board of the Faculty of Medicine, University of Tokyo (approval number: 2019010NI-16) and the Gunma Children's Medical Center (approval number: GCMC2023-21) and was conducted in accordance with the Declaration of Helsinki. Because previously stored specimens were used, informed consent could not be obtained. Therefore, an opt-out approach was implemented by publicly disclosing study information and providing participants with the opportunity to decline participation as an alternative to written informed consent.

Patient background

Proteomic analysis was performed on 45 FFPE samples obtained from 15 patients (mean age, 6.5 ± 3.3 months; male-to-female ratio, 11:4), including specimens from recto-sigmoid and long-segment aganglionic regions (Supplementary Table 1).

Preparation of FFPE specimens

Specimens collected during surgery were immediately immersed in 10% neutral-buffered formalin and fixed for at least 24 h. After fixation, the tissues were washed under running water for 30 min, trimmed, enclosed in cassettes, and re-immersed in formalin. The tissue cassettes were then washed again under running water for 30 min before paraffin infiltration using a paraffin processing system (Tissue-Tek VIP6; Sakura Finetek Japan Co., Ltd.). Finally, the specimens were embedded using an embedding system

(Tissue-Tek TEC5 Embedding Module and Cryo Module; Sakura Finetek Japan Co., Ltd.) and sectioned at a thickness of 10μm for proteome analysis.

Sample preparation for proteomic analysis

Protein extraction was performed by reversing formaldehyde-induced cross-links between proteins in the FFPE samples. Briefly, FFPE samples were immersed in 1 mL of PathoClean (FUJIFILM Wako Pure Chemical Corporation, Osaka, Japan) and rotated for 30 min. The mixture was then centrifuged at 15,000 g for 15 min, and the supernatant was removed. Ethanol (1 mL) was added to the remaining pellet, and the mixture was rotated for 30 min. After centrifugation at 15,000 g for 5 min, the supernatant was discarded. Subsequently, 125 μL of 1 M Tris (pH 8.0) and 125 μL of 10% sodium dodecyl sulfate were added to the pellet, followed by incubation at 95°C for 120 min. After incubation, the mixture was sonicated using BIORUPTOR BR-II (SONIC BIO Co., Kanagawa, Japan) for 30 min and centrifuged at 15,000g for 15 min. The resulting supernatant was collected as the extracted protein fraction.

Protein concentration was quantified using the Pierce™ BCA Protein Assay Kit (Thermo Fisher Scientific, WA, USA) and adjusted to 200 ng/μL. Protein purification (40 μg) and digestion were performed using the SP3-LASP method.[5,6] Tryptic digestion was performed using 500 ng/μL Trypsin Platinum (Promega, Madison, WI, USA) for 14 h at 37°C. The digested samples were reduced and alkylated by adding 8 μL of 110 mM tris(2-carboxyethyl) phosphine and 440 mM 2-chloroacetamide, followed by incubation at 80°C for 15 min. The samples were then acidified with 16 μL of 5% trifluoroacetic acid. The digested peptides were purified using GL-Tip SDB (GL Sciences, Tokyo, Japan) according to the manufacturer's protocol. The purified peptides were redissolved in 0.02% decyl maltose neopentyl glycol containing 0.1% trifluoroacetic acid, quantified using the Pierce Quantitative Fluorescent Peptide Assay Kit (Thermo Fisher Scientific), and adjusted to 50 ng/μL.

Liquid chromatography–tandem mass spectrometry analysis

The digested peptides (250 ng) were directly loaded onto a 75 μm × 30 cm nanoLC nano-capillary column (C18, particle size 1.7 μm, 100 Å; CoAnn Technologies, Richland, WA, USA) maintained at 50°C. Peptides were separated using a 100-min gradient with mobile phase A (0.1% formic acid in water) and mobile phase B (0.1% formic acid in 80% acetonitrile) at a flow rate of 150 nL/min using an UltiMate 3000 RSLCnano LC system (Thermo Fisher Scientific). The gradient conditions were as follows: 0 min, 7% B; 86 min, 37% B; 93 min, 70% B; and 100 min, 70% B. The eluted peptides were analyzed using an Orbitrap Exploris 480 mass spectrometer (Thermo Fisher Scientific) equipped with an InSpIon system.[7] The MS1 scan range was set to 495–745 m/z at a resolution of 60,000, with an automatic gain control target set to 3×10^6 and maximum injection time set to "auto." MS2 spectra were acquired over the range of 200–1,800 m/z at a resolution of 45,000, with an automatic gain control target of 3×10^6, maximum injection time set to "auto," and a fixed normalized collision energy of 26%. The MS2 isolation

width was set to 4 Th, and an optimized window arrangement was used for the 500–740 m/z window pattern in Xcalibur 4.4 (Thermo Fisher Scientific).

Data analysis

Data-independent acquisition (DIA)-NN v1.9.1 was used to analyze DIA-MS data against an in silico human spectral library (https://github.com/vdemichev/DiaNN).[8] First, a spectral library was generated using the human protein sequence database from UniProt (proteome ID: UP000005640; 20,598 entries; downloaded on April 1, 2024) with DIA-NN. The parameters used for spectral library generation were as follows: digestion enzyme, trypsin; maximum missed cleavages, 1; peptide length range, 7–45 amino acids; precursor charge range, 2–4; precursor mass range, 500–740 m/z; and fragment ion m/z range, 200–1,800. The options "FASTA digest for library-free search/library generation," "deep learning-based spectra, RTs and IM prediction," and "n-term M excision" were enabled. The following parameters were used for protein and precursor identification: mass accuracy, 10 ppm; MS1 accuracy, 10 ppm; protein inference, genes; neural network classifiers, single-pass mode; quantification strategy, QuantUMS (high precision); and cross-run normalization, RT-dependent. The additional algorithms "Unrelated runs," "Peptideforms," "Heuristic protein inference," and "No shared spectra" were enabled. Protein identification was performed using a false discovery rate threshold of ≤ 1% at both the precursor and protein levels. Protein quantification values were calculated using the default DIA-NN settings.

Missing values for undetected proteins were imputed by sampling from a normal distribution, with the median shifted toward lower abundance relative to the distribution of detected proteins (downshift, 1.8; width, 0.3).[9] Protein abundance levels were $\log_{10}$-transformed. Principal component analysis was performed using the prcomp function in R (v4.5.1).

Differential protein abundance was assessed using the limma package (v3.64.3).[10] Linear models were fitted to the log-transformed protein abundance data, with region (AS, TZ, and NI) included as the main factor and sex as a covariate. To account for within-patient correlations resulting from multiple samples obtained from the same individual, the duplicateCorrelation approach was applied, with patient ID included as a blocking factor. Empirical Bayes moderation was used to improve variance estimation. Pairwise group comparisons were performed, and p-values were adjusted for multiple testing using the Benjamini–Hochberg method. Proteins with an adjusted p-value < 0.05 were considered statistically significant. Heatmaps were generated using the pheatmap package (v1.0.13).

Gene set enrichment analysis (GSEA) was performed using the gseGO function in the clusterProfiler package (v4.16.0) with the fgsea algorithm.[11] Proteins were ranked according to signed $-\log_{10}$-transformed p-values incorporating the direction of fold change. Enrichment analysis was performed for Gene Ontology Biological Process terms, with significance defined as a Benjamini–Hochberg-adjusted p-value < 0.05.

Immunohistochemistry

Immunohistochemical staining was performed on FFPE tissue sections cut to a thickness of 3 μm, as previously described.[3] Primary antibodies against catenin alpha-2 (CTNNA2; 14362-1-AP, 1:1,000; Proteintech, Rosemont, IL, USA), mammalian ependymin-related protein 1 (EPDR1; HPA072321, 1:650; Sigma-Aldrich), NAC-alpha domain-containing protein 1 (NACAD; HPA020981, 1:25; Sigma-Aldrich), neural cell adhesion molecule 2 (NCAM2; HPA030900, 1:500; Sigma-Aldrich), and nitric oxide synthase 1 (NOS1; HPA069509, 1:550; Sigma-Aldrich) were applied. Visualization was performed using a commercial biotin–streptavidin immunoperoxidase kit (Histofine; Nichirei, Tokyo, Japan) and 3,3'-diaminobenzidine.

Results

Proteomic analysis of FFPE samples

Our study demonstrated the successful application of proteomic analysis to pathological specimens that were not originally intended for such analyses. These findings suggest that DIA-based proteomic analysis of FFPE samples has substantial potential as a minimally invasive approach for detecting and analyzing proteins from small tissue specimens and may facilitate elucidation of the pathogenesis of pediatric surgical diseases such as HSCR. We performed DIA proteomic analysis, a highly effective method for protein quantification from various human-derived sources in clinical research, using 45 FFPE samples obtained from 15 patients. The analysis identified 10,541 human-derived proteins, of which 9,563 proteins detected in at least 20 samples were retained for subsequent analyses according to criteria established in our previous studies.[3,12,13]

Principal component analysis of the FFPE proteome

Principal component analysis revealed that protein expression profiles were more strongly associated with inter-individual variation than with anatomical location (Supplementary Fig. 1). These findings suggest that variability in proteomic profiles is driven predominantly by individual-specific characteristics rather than HSCR-related features.

Comparative proteomic analysis: protein differences across anatomical regions

Among the 9,563 proteins analyzed, comparison between the NI and TZ groups identified 70 proteins with significant differential expression (Fig. 1), whereas 606 proteins differed significantly between the NI and AS groups. A total of 13 proteins, including calretinin, cadherin-2, collapsin response mediator protein 1, CTNNA2, EPDR1, alpha-internexin, neural cell adhesion molecule L1, microtubule-associated protein 2, microtubule-associated protein 6, NACAD, NCAM2, nitric oxide synthase 1, and peripherin, were significantly upregulated in the NI group (Table 1). Among these proteins, CTNNA2, EPDR1, NACAD,

and NCAM2 have not previously been associated with HSCR or intestinal development. Therefore, these four proteins were selected for further evaluation (Fig. 2).

Table 1. Proteins significantly upregulated in the normal intestine compared with the transitional zone and aganglionic segment.

	Master Protein Name	Master Gene Symbol	Log FC	*p-value*	adj. *p-value*
1	Calretinin	CALB2	-0.2464294	9.65E-07	0.00089454
2	Cadherin-2	CDH2	-0.1612328	0.00021867	0.03544228
3	Dihydropyrimidinase-related protein 1	CRMP1	-0.1992595	4.24E-07	0.00057958
4	Catenin alpha-2	CTNNA2	-0.3065611	1.22E-07	0.00023356
5	Mammalian ependymin-related protein 1	EPDR1	-0.0790952	0.00017517	0.03045704
6	Alpha-internexin	INA	-0.3270426	1.49E-07	0.0002376
7	Neural cell adhesion molecule L1	L1CAM	-0.2985717	6.80E-06	0.00271396
8	Microtubule-associated protein 2	MAP2	-0.1524352	1.36E-05	0.00447343
9	Microtubule-associated protein 6	MAP6	-0.311832	2.40E-09	7.65E-06
10	NAC-alpha domain-containing protein 1	NACAD	-0.1450552	1.02E-05	0.00359879
11	Neural cell adhesion molecule 2	NCAM2	-0.21871	3.85E-06	0.00183953
12	Nitric oxide synthase 1	NOS1	-0.2092738	8.37E-07	0.00089454
13	Peripherin	PRPH	-0.2926575	2.39E-05	0.00671151

Log fold change (logFC), p-values, and adjusted p-values are presented for the comparison between the normal intestine and transitional zone groups.

Gene set enrichment analysis

To characterize molecular differences across anatomical regions affected by HSCR, we performed GSEA. The analysis demonstrated significant upregulation of neuron-related protein sets in the NI compared with the AS and TZ. Specifically, pathways associated with neuron projection morphogenesis, regulation of trans-synaptic signaling, modulation of chemical synaptic transmission, synaptic signaling, trans-synaptic signaling, antegrade trans-synaptic signaling, and chemical synaptic transmission were enriched in the NI region (Fig. 3a, b). Similarly, pathways related to neuronal development, including neuron projection morphogenesis and cell morphogenesis involved in neuron differentiation, were enriched in the TZ compared with the AS (Fig. 3c). These findings are consistent with the known clinical and pathological characteristics of HSCR.

Immunohistochemistry

Among the 13 identified proteins, we focused on four proteins—CTNNA2, EPDR1, NACAD, and NCAM2—that have not previously been investigated in relation to HSCR or gastrointestinal development, with the aim of identifying novel intraoperative diagnostic biomarkers for HSCR. To validate the proteomic findings, immunohistochemical staining for these four proteins was performed in tissue samples from patients with HSCR. All four proteins and NOS1 demonstrated positive staining restricted to ganglionic regions of the large intestine (Fig. 4). In contrast, little to no staining was observed in the TZ or AS, consistent with the decreased density or absence of ganglion cells in these regions, as confirmed by NACAD staining (Fig. 5).

Discussion

Although molecular biomarkers for HSCR, such as calretinin,[14–16] S100, and peripherin,[17,18] are already used in clinical practice, no definitive intraoperative diagnostic method for HSCR has yet been established. This limitation partly reflects the rarity of HSCR, which restricts the feasibility of large cohort studies because of the limited number of affected patients. In addition, many previous investigations have adopted a bottom-up approach focused on previously recognized molecules and pathways.[18]

FFPE tissue is the most widely used method for preserving resected specimens in surgical practice.[1] Over the years, FFPE samples have been extensively accumulated in medical institutions worldwide, making them an invaluable resource for research, and quantitative analyses using FFPE specimens have been performed for more than two decades.[19] Importantly, the ability to conduct studies using archived FFPE specimens without subjecting pediatric patients to additional invasive procedures represents a major advancement.[3] Further development of this approach may provide critical insights into the pathophysiology of various pediatric surgical diseases. Moreover, FFPE-based proteomic analysis enables a top-down approach for investigating rare pediatric diseases.

In this study, we performed extensive proteomic analysis of FFPE samples from 15 patients to identify novel diagnostic biomarkers for HSCR. We identified 13 proteins that were significantly upregulated in the NI compared with the AS and TZ. Among these proteins, calretinin, microtubule-associated protein 2, nitric oxide synthase 1(NOS1), and peripherin have previously been associated with HSCR.[17,18,20,21] In addition, cadherin-2, collapsin response mediator protein 1, alpha-internexin, neural cell adhesion molecule L1, and microtubule-associated protein 6 have been implicated in gastrointestinal development.[22–25] GSEA further demonstrated enrichment of neuron-related protein sets in the NI group compared with the TZ and AS groups. These findings are consistent with the known clinical and pathological characteristics of HSCR and further support the validity of our FFPE-based proteomic analysis.

We subsequently focused on CTNNA2, EPDR1, NACAD, and NCAM2 because these proteins have not previously been associated with HSCR or gastrointestinal development and therefore represent potential novel intraoperative biomarkers for HSCR. Immunohistochemical analysis validated the proteomic findings, demonstrating positive staining for all four proteins restricted to ganglionic regions of the large intestine, whereas minimal or no staining was observed in the TZ or AS. These findings suggest potential clinical utility for these proteins as intraoperative diagnostic markers, particularly for identifying ganglionic bowel during HSCR surgery.

This study has several limitations. First, the sample size was relatively small, reflecting the pilot nature of this study. Second, intraoperative analyses using frozen sections were not performed because of limitations in the study design. Nevertheless, our top-down approach using proteomic analysis represents an important first step toward biomarker discovery for rare diseases. Furthermore, our

findings may provide valuable insights for the development of an intraoperative diagnostic method for HSCR.

Conclusions

To the best of our knowledge, this study is the first to apply comprehensive proteomic analysis to FFPE specimens from patients with HSCR in the field of pediatric surgery. FFPE-based proteomics has the potential to advance our understanding of the pathophysiology of not only HSCR but also other rare pediatric disorders. Future multicenter studies involving larger patient cohorts and intraoperative validation are warranted to confirm these findings and support the development of reliable intraoperative diagnostic methods for HSCR.

Abbreviations

Hirschsprung disease
HSCR
formalin-fixed
paraffin-embedded,FFPE
aganglionic segment
AS
transitional zone
TZ
normal intestine
NI
catenin alpha-2
CTNNA2
mammalian ependymin-related protein 1
NACAD
neural cell adhesion molecule 2
EPDR1
neural cell adhesion molecule 2
NCAM2
data-independent acquisition
DIA
gene set enrichment analysis
GSEA
nitric oxide synthase 1
NOS1

Declarations

Ethics approval and consent to participate

This study was approved by the Institutional Review Board of the Faculty of Medicine, University of Tokyo (approval number: 2019010NI-16) and the Gunma Children's Medical Center (approval number: GCMC2023-21) and was performed in compliance with the Declaration of Helsinki. Since previously stored specimens were used, informed consent could not be obtained; therefore, an opt-out method was employed by disclosing information and providing an opportunity to refuse, as a substitute for obtaining consent.

Competing interests

The authors declare no conflict of interests.

Funding

This work was supported by the Japan Society for the Promotion of Sciences through Grants-in-Aid for Scientific Research (grant numbers: 23K15465 and 23K17424) and by the Kawano Masanori Public Interest Incorporated Foundation for Promotion of Pediatrics.

Author Contribution

Conceptualization: E.W.; methodology: E.W., and Y.K.; software: E.W., M.Y., R.K. and Y.K.; validation: E.W., S.K., M.Y., and Y.K.; formal analysis: E.W., M.Y., and Y.K.; investigation: E.W., S.K., M.Y., A.Y., R.K., and Y.K.; resources: E.W., S.K., S.T., A.N., and J.F.; data curation: E.W., S.K., M.Y., and Y.K.; writing—original draft preparation: E.W., S.K., A.Y., M.Y., R.K., and Y.K.; writing—review and editing: E.W., S.K., A.Y., M.Y., R.K., O.O., and Y.K.; visualization: E.W. and M.Y.; supervision: O.O.; project administration: E.W.; funding acquisition: E.W.

All authors approved the final manuscript and consented to its publication.

Acknowledgement

The authors express their sincere appreciation to Dr. Junko Hirato for the pathological analysis.

Availability of data and materials

Mass spectrometry proteomic data are deposited in the ProteomeXchange Consortium via the jPOST partner repository (dataset identifiers: PXD081012 for ProteomeXchange and JPST004761 for jPOST). Data are available at the following links but are only accessible via access keys: 8057.

https://repository.jpostdb.org/preview/9217684176a55b79def467

References

1. Buczak K, Kirkpatrick JM, Truckenmueller F, et al. Spatially resolved analysis of FFPE tissue proteomes by quantitative mass spectrometry. Nat Protoc. 2020;15:2956–79. https://doi.org/10.1038/s41596-020-0356-y.
2. Eckert TüshausJ, Schliemann S, M., et al. Towards routine proteome profiling of FFPE tissue: insights from a 1,220-case pan-cancer study. EMBO J. 2025;44:304–29. https://doi.org/10.1038/s44318-024-00289-w.
3. Shinohara M, Ishikawa M, Yoshihara M, et al. Proteome analysis of preserved formalin-fixed and paraffin-embedded specimens to explore the pathogenesis of infantile hypertrophic pyloric stenosis. Pediatr Surg Int. 2025;41:262. https://doi.org/10.1007/s00383-025-06153-0.
4. Montalva L, Cheng LS, Kapur R, et al. Hirschsprung disease. Nat Rev Dis Primers. 2023;9:54. https://doi.org/10.1038/s41572-023-00465-y.
5. Konno R, Ishikawa M, Nakajima D, Endo Y, Ohara O, Kawashima Y. Universal pretreatment development for low-input proteomics using Lauryl maltose neopentyl glycol. Mol Cell Proteom. 2024;23:100745. https://doi.org/10.1016/j.mcpro.2024.100745.
6. Konno R, Ishikawa M, Nakajima D, Inukai K, Ohara O, Kawashima Y. Thin-diaPASEF: diaPASEF for maximizing proteome coverage in single-shot proteomics. DNA Res. 2025;32:dsaf019. https://doi.org/10.1093/dnares/dsaf019.
7. Kawashima Y, Ishikawa M, Konno R, Nakajima D, Ohara O. Development of a simple and stable NanoESI spray system using suction wind from the MS inlet. J Proteome Res. 2023;22:1564–9. https://doi.org/10.1021/acs.jproteome.3c00146.
8. Demichev V, Messner CB, Vernardis SI, Lilley KS, Ralser M. DIA-NN: neural networks and interference correction enable deep proteome coverage in high throughput. Nat Methods. 2020;17:41–4. https://doi.org/10.1038/s41592-019-0638-x.
9. Tyanova S, Temu T, Sinitcyn P, et al. The Perseus computational platform for comprehensive analysis of (prote)omics data. Nat Methods. 2016;13:731–40. https://doi.org/10.1038/nmeth.3901.
10. Ritchie ME, Phipson B, Wu D, et al. limma powers differential expression analyses for RNA-sequencing and microarray studies. Nucleic Acids Res. 2015;43:e47. https://doi.org/10.1093/nar/gkv007.
11. Wu T, Hu E, Xu S, et al. clusterProfiler 4.0: a universal enrichment tool for interpreting omics data. Innovation. 2021;2:100141. https://doi.org/10.1016/j.xinn.2021.100141.
12. Shitara Y, Konno R, Yoshihara M, et al. Host-derived protein profiles of human neonatal meconium across gestational ages. Nat Commun. 2024;15:5543. https://doi.org/10.1038/s41467-024-49805-w.

13. Watanabe E, Saito T, Yoshihara M, et al. Assessing native liver post-Kasai portoenterostomy for biliary atresia through stool proteome analysis. Gastro Hepatol Adv. 2025;4:100688. https://doi.org/10.1016/j.gastha.2025.100688.
14. Guinard-Samuel V, Bonnard A, De Lagausie P, et al. Calretinin immunohistochemistry: a simple and efficient tool to diagnose Hirschsprung disease. Mod Pathol. 2009;22:1379–84. https://doi.org/10.1038/modpathol.2009.110.
15. Kapur RP, Reed RC, Finn LS, Patterson K, Johanson J, Rutledge JC. Calretinin immunohistochemistry versus acetylcholinesterase histochemistry in the evaluation of suction rectal biopsies for Hirschsprung disease. Pediatr Dev Pathol. 2009;12:6–15. https://doi.org/10.2350/08-02-0424.1.
16. Barshack I, Fridman E, Goldberg I, Chowers Y, Kopolovic J. The loss of calretinin expression indicates aganglionosis in Hirschsprung's disease. J Clin Pathol. 2004;57:712–6. https://doi.org/10.1136/jcp.2004.016030.
17. Holland SK, Hessler RB, Reid-Nicholson MD, Ramalingam P, Lee JR. Utilization of peripherin and S-100 immunohistochemistry in the diagnosis of Hirschsprung disease. Mod Pathol. 2010;23:1173–9. https://doi.org/10.1038/modpathol.2010.104.
18. Claxton HL, Lounis SA, Stanton M, Hall NJ, Aldeiri B. The diagnostic value of immunohistochemistry markers in Hirschsprung disease; a systematic review and meta-analysis. J Pediatr Surg. 2025;60:162010. https://doi.org/10.1016/j.jpedsurg.2024.162010.
19. Coscia F, Doll S, Bech JM, et al. A streamlined mass spectrometry-based proteomics workflow for large-scale FFPE tissue analysis. J Pathol. 2020;251:100–12. https://doi.org/10.1002/path.5420.
20. Chisholm KM, Longacre TA. Utility of peripherin versus MAP-2 and calretinin in the evaluation of Hirschsprung disease. Appl Immunohistochem Mol Morphol. 2016;24:627–32. https://doi.org/10.1097/PAI.0000000000000241.
21. Eisenberg JD, Bradley RP, Graham KD, et al. Three-dimensional imaging of the enteric nervous system in human pediatric colon reveals new features of Hirschsprung's disease. Gastroenterology. 2024;167:547–59. https://doi.org/10.1053/j.gastro.2024.02.045.
22. Heanue TA, Pachnis V. 2006, Expression profiling the developing mammalian enteric nervous system identifies marker and candidate Hirschsprung disease genes, Proc. Natl. Acad. Sci. USA., 103, 6919–6924. https://doi.org/10.1073/pnas.0602152103
23. Rauch U, Klotz M, Maas-Omlor S, et al. Expression of intermediate filament proteins and neuronal markers in the human fetal gut. J Histochem Cytochem. 2006;54:39–46. https://doi.org/10.1369/jhc.4A6495.2005.
24. Fernández RM, Núñez-Torres R, García-Díaz L, de Agustín JC, Antiñolo G, Borrego S. Association of X-linked hydrocephalus and Hirschsprung disease: report of a new patient with a mutation in the L1CAM gene, Am. J Med Genet A. 2012;158A:816–20. https://doi.org/10.1002/ajmg.a.35244.
25. Broders-Bondon F, Paul-Gilloteaux P, Carlier C, Radice GL, Dufour S. N-cadherin and beta1-integrins cooperate during the development of the enteric nervous system. Dev Biol. 2012;364:178–91. https://doi.org/10.1016/j.ydbio.2012.02.001.

Figures

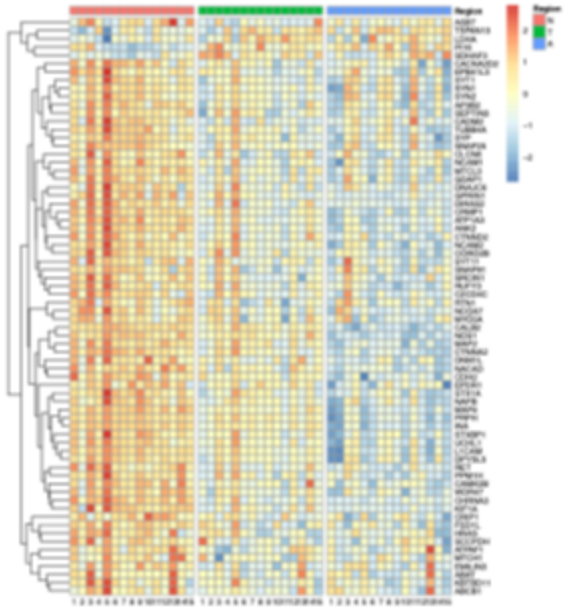


Figure 1

Heatmap of 70 proteins showing significant differential expression between the normal intestinal segment (N) and transitional zone (T).

A, aganglionic segment.

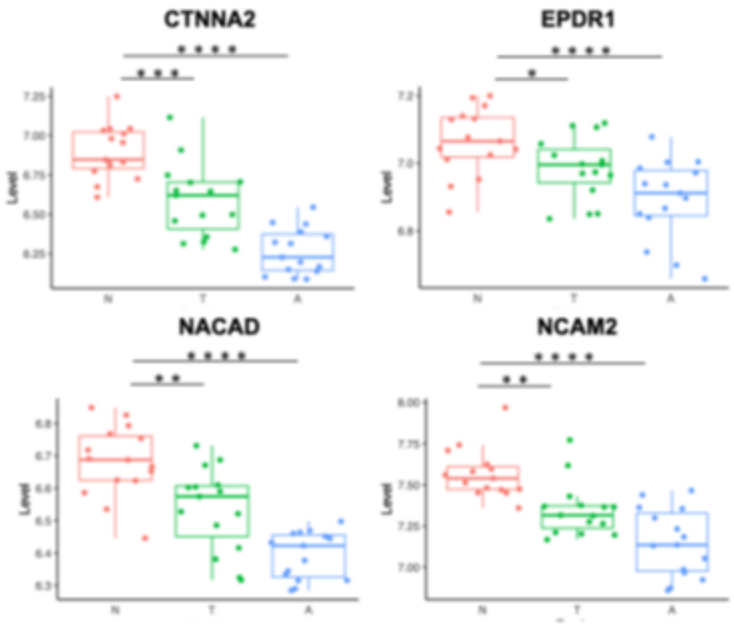


Figure 2

Comparative expression of four proteins specifically upregulated in the normal intestinal segment.

N, normal intestine; T, transitional zone; A, aganglionic segment.

Adjusted p-values: *p < 0.05, **p < 0.01, ***p < 0.001, ****p < 0.0001.

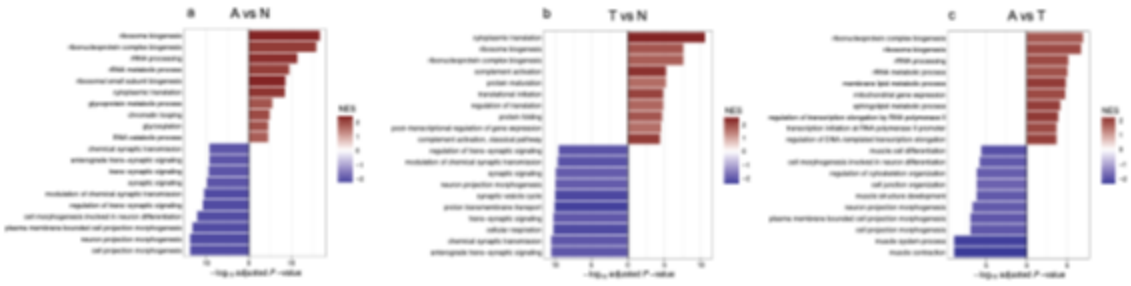


Figure 3

Gene set enrichment analysis (GSEA) of proteomic data across anatomical regions.

Bar plots showing the top 10 significantly enriched Gene Ontology terms for proteins enriched in: (a) the aganglionic segment (A, red) and normal intestine (N, blue); (b) the transitional zone (T, red) and normal intestine (N, blue); and (c) the aganglionic segment (A, red) and transitional zone (T, blue). NES refers to the normalized enrichment score. All p-values were calculated using permutation testing with Benjamini–Hochberg correction based on the GSEA algorithm implemented in fgsea.

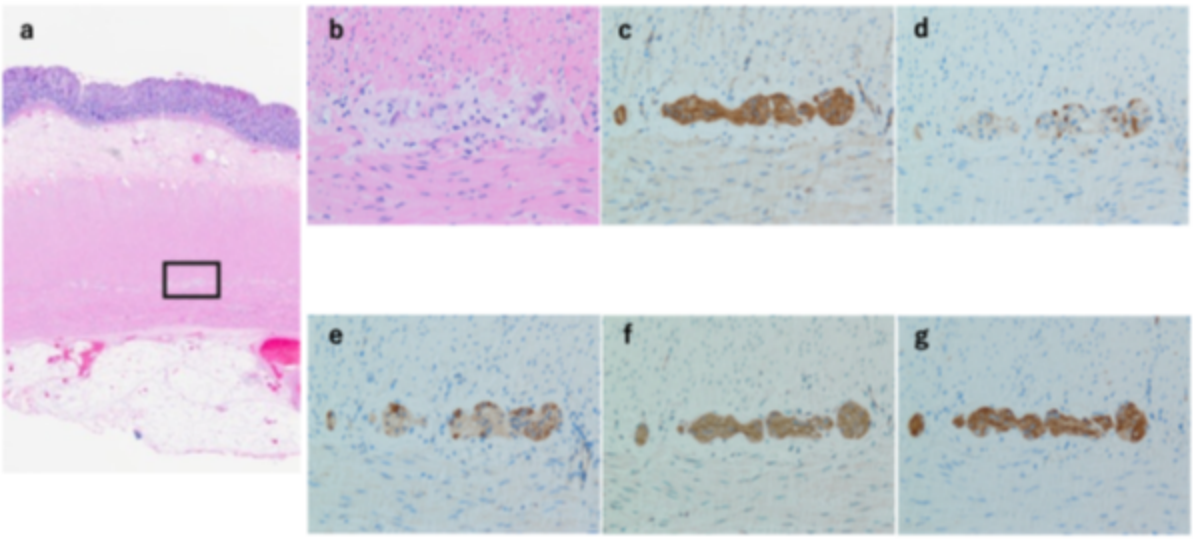


Figure 4

Hematoxylin and eosin staining and immunohistochemistry for CTNNA2, EPDR1, NACAD, NCAM2, and NOS1 in the uninvolved segment of Patient 10. (a, b) Hematoxylin and eosin staining demonstrating Auerbach's plexus located between the muscle layers, with ganglion cells present within the plexus. (c) CTNNA2; (d) EPDR1; (e) NACAD; (f) NCAM2; (g) NOS1. Immunohistochemistry demonstrated varying degrees of positivity in ganglion cells depending on the antibody used. Panel (a) shows a virtual semi-macro image derived from whole-slide imaging. Original magnification: panels (b–g), ×200.

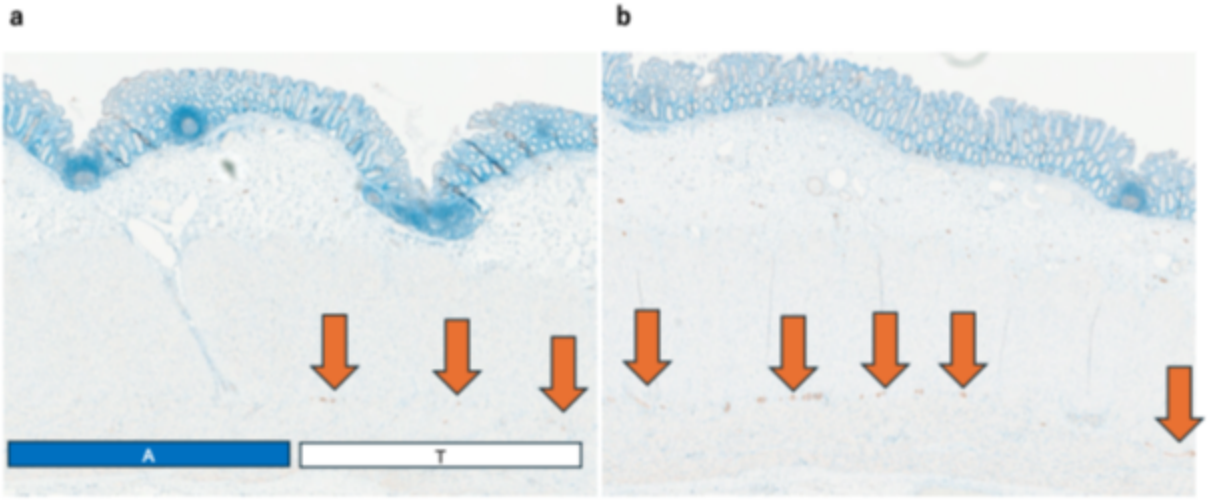


Figure 5

Virtual semi-macro image derived from whole-slide NACAD staining of Patient 10.

(a) In the aganglionic segment (A, blue bars), ganglion cells are absent from the myenteric plexus and show no immunoreactivity, whereas NACAD-positive ganglion cells (arrows) are present in the transitional zone (T). (b) In the normal intestine, Auerbach’s plexus is located between the muscle layers, with ganglion cells present within the plexus.

Supplementary Files

This is a list of supplementary files associated with this preprint. Click to download.

- SupplementaryTablesFigures.docx